Acta Biomaterialia 97 (2019) 623–636

Contents lists available at ScienceDirect

Acta Biomaterialia

journal homepage: www.elsevier.com/locate/actabiomat

Full length article

In vitro and in vivo studies on magnesium alloys to evaluate the feasibility of their use in obstetrics and gynecology

Guo Bao [a,b], Qianqian Fan [a], Dongfeng Ge [a], Mingming Sun [a], Hui Guo [c], Dandan Xia [c], Yang Liu [c], Jianing Liu [c], Shangchun Wu [b], Bin He [b,*], Yufeng Zheng [a,c,*]

[a] Graduate School of Peking Union Medical College, Beijing 100730, China
[b] Department of Reproduction and Physiology, National Research Institute for Family Planning, Beijing 100081, China
[c] Department of Materials Science and Engineering, College of Engineering, Peking University, Beijing 100871, China

ARTICLE INFO

Article history:
Received 22 March 2019
Received in revised form 15 July 2019
Accepted 1 August 2019
Available online 03 August 2019

Keywords:
Magnesium alloys
Biodegradable metals
Intrauterine microenvironment
Simulated uterine fluid
Obstetrics and gynecology

ABSTRACT

Magnesium and its alloys were widely investigated in many body fluid microenvironments including bone, blood, bile, saliva, and urine; however, no study has been conducted in the intrauterine microenvironment. In this study, the degradation behaviors of HP-Mg, Mg-1Ca, and Mg-2Zn alloys in simulated uterine fluid (SUF) were systematically investigated, and then the biological response of four kinds of uterine cells to these materials was observed. For this purpose, the gluteal muscle of rat was used as the implantation position to study the in vivo biocompatibility as a mimic of the intrauterine device (IUD) fixation part. The 120-day immersion test indicated that the Mg-1Ca alloy had a faster degradation rate than the Mg-2Zn alloy and HP-Mg and dissolved entirely in the SUF. Indirect cytotoxicity assay showed that the extracts of HP-Mg, Mg-1Ca, and Mg-2Zn alloys have positive effects on human uterine smooth muscle cells (HUSMC), human endometrial epithelial cells (HEEC), and human endometrial stromal cells (HESC), especially for the Mg-1Ca alloy group. Furthermore, the in vivo experiment showed that HP-Mg, Mg-1Ca, and Mg-2Zn alloy implants cause a light inflammatory response in the initial 3 days, but they were surrounded mainly by connective tissue, and lymphocytes were rarely observed at 4 weeks. Based on the above facts, we believed that it is feasible for using biomedical Mg alloys in obstetrics and gynecology and proposed three kinds of medical device candidates for future R&D.

Statement of Significance

Magnesium alloys were widely investigated in various body microenvironments including bone, blood, bile, saliva, and urine; however, no study has been conducted in the intrauterine environment. In this work, the degradation behaviors of Mg alloys in simulated uterine fluid were systematically investigated, and then the biological response of four kinds of uterine cells to these materials was observed. For this purpose, the tibialis anterior of a rat model was used as the implantation position to study the in vivo biocompatibility. The comprehensive in vitro and in vivo testing results indicated that biomedical Mg alloys are feasible for use in obstetrics and gynecology. Further, three kinds of medical device candidates were proposed.

1. Introduction

As degradable metallic biomaterials, magnesium and its alloys have received much attention in the past 10 years [1–7]. The main focuses were bone fixation devices, biliary, esophageal and cardiovascular stents, and tissue-engineered scaffolds; the majority of in vitro and in vivo studies involved physiological microenvironments such as bone, blood, bile, saliva, and urine [8–12]. In 2013, a magnesium-based screw devoted to bone fixation received Conformity European (CE) mark approval for class III medical device [13], and in 2016, a magnesium-based drug-eluting stent received CE mark approval for obstructive coronary disease [14]. To date, there is no report on the feasibility of using magnesium and its alloys in obstetrics and gynecology.

For in vitro biocompatibility study, different simulated body fluids (SBFs) and cell lines were employed to mimic different physiological micro-environments. (1) *Skeletal musculature:* SBF is used to simulate the orthopedic environment in bone research, and L929

* Corresponding authors at: Department of Materials Science and Engineering, College of Engineering, Peking University, No.5 Yi-He-Yuan Road, Hai-Dian District, Beijing 100871, China (Y. Zheng).

E-mail addresses: hebin@nrifp.org.cn (B. He), yfzheng@pku.edu.cn (Y. Zheng).

https://doi.org/10.1016/j.actbio.2019.08.001
1742-7061/

and MG63 cells are used to evaluate the cytocompatibility of materials [15–20]. (2) *Hematological system:* In the study of vascular stents, Hank's solution was used as the corrosive medium. Vascular smooth muscle cells (VSMC), vascular endothelial cells (VEC), and umbilical vein epithelial cells (UVEC) were used to evaluate the cytocompatibility of the materials [21–23]. (3) *Digestive system:* Simulated saliva was used to evaluate the degradable behavior of esophageal stents, and esophageal epithelial cells were used to assess the biocompatibility of materials [10]. (4) *Urinary system:* In the related study of urethral stents, simulated urine was used as the corrosive medium of the materials [24]. Urinary epithelial cells were used to evaluate the biocompatibility of the materials [25]. Thus far, the results of existing studies showed that the degradation rate and degradation products of magnesium alloys were different because of different chemical reactions with body fluids in various physiological environments.

Intrauterine device (IUD) has been extensively studied as a medical device implanted into the uterine environment of the human body [26,27], such as GyneFix®, which contains a fixed device for postpartum [28]. The fixing device is made of a poly (DL-lactide-co-glycolide) (PDLGA) material. However, its limitation is the strong hygroscopicity, low heat stability, and poor flexibility to elongate. As the strength of the fixation part, which is made of polymers, is not strong enough, it has to be built into a large cone. Another medical equipment commonly used in the uterus is the polymer balloon uterine stent (Cook Medical). This stent is implanted inside the uterus immediately after surgery for intrauterine adhesions (IUA) because it can conform to the cavity of a normal uterus and maintain separation at the margins of the uterine cavity; this stent was placed for 1 month after hysteroscopic adhesiolysis to prevent adhesion reformation[29,30]. Considering the degradation characteristics of magnesium and its alloys, the uterus may be a potentially applicable organ for the above-mentioned applications. However, there has been no report concerning the effects of magnesium and its alloys on the cells in the uterine micro-environment by cell culture and in regions surrounding the uterine tissue by animal testing. In the uterine tissue, human endometrial epithelial cells (HEEC), human endometrial stromal cells (HESC), and human uterine smooth muscle cells (HUSMC) are important to maintain the tissue micro-environment. Presently, most of the related studies on the uterine environment use simulated uterine fluid (SUF) [26,31] to carry out related experiments in vitro. In the evaluation of IUD, HEEC were used for related cellular descriptive experiments [32]. Their response to materials plays a crucial role in the future application of magnesium alloys in the intrauterine environment.

In this work, the degradation behaviors of HP-Mg, Mg-1Ca, and Mg-2Zn alloys in SUF were systematically investigated to determine its performance in the intrauterine environment through electrochemical tests; immersion corrosion experiments; and scanning electron microscopy (SEM), energy-dispersive spectroscopy (EDS), and X-ray diffraction (XRD), and cell proliferation experiments to detect cytocompatibility. Later on, the materials were implanted into the animal model, and H&E staining was adopted to assess histocompatibility.

2. Experimental details

2.1. Material preparation

Magnesium alloy ingots with the nominal composition of Mg-1Ca and Mg-2Zn (wt.%) were prepared from commercial pure Mg (99.99%), pure Ca (99.95%), and pure Zn (99.99%) in a crucible, then they were hot extruded into rod samples with an extrusion ratio of 11. Details about material preparation can be found in our previous publication [33]. The raw ingot of HP-Mg was purchased from Hebi Wuhua Magnesium Processing Co. Ltd., China and then extruded with a reduction ratio of 12 at 320 °C. All experimental rods were cut into samples with 10 mm diameter and 2 mm thickness, polished with SiC papers with granulations from 800 to 2000 grit, then cleaned ultrasonically in absolute ethanol for 15 min, and, finally, air-dried.

2.2. Immersion tests

Static immersion tests were carried out in SUF (NaCl 4.97 g/L, KCl 0.224 g/L, $CaCl_2$ 0.167 g/L, $NaHCO_3$ 0.25 g/L, Glucose 0.50 g/L, $NaH_2PO_4 \cdot 2H_2O$ 0.072 g/L; Table 1 shows the concentration of ions and other components in SUF and other SBFs) according to ASTM-G31-72 at 37 °C in a water bath lasting for up to 120 days, with a ratio of solution volume to sample surface area (V/S) at 20 mL/cm^2. During the immersion test, the SUF solution remained unchanged and was not replaced. A previous study proved that, in Hank's solution, the corrosion rates of HP Mg, AZ91, and ZE41 decreased with increasing pH value [34], which means that different pH values and solution compositions can also have an impact on corrosion rates and the formation of corrosion products. Reported values for the pH of human uterine solutions vary from 6.0 to 7.9 with the female menstrual physiological cycle [35–37]. Therefore, in this study, we set 6.0, 7.0, and 7.9 as the initial pH of the SUF and monitored the change in pH values of the samples from 1 to 10, 15, 20, 25, 30, 35, 42, 90, and 120 days. After 10, 42, and 120 days, some samples were taken out of the solution, gently rinsed with distilled water, and subsequently air-dried. Then corrosion products on the surface of the samples were removed with chromic acid (200 g/L CrO_3 + 10 g/L $AgNO_3$) for 5 min at room temperature. The degradation rate was determined using the following equation:

$$C = \frac{\Delta m}{\rho \times A \times t}$$

where C is the corrosion rate in mm/year, Δm is the reduction in weight, ρ is the density of the material, A is the initial implant surface area, and t is the implantation time. At least four measurements were taken for each group.

2.3. Surface characterization

Surface characterization of the samples was performed using a scanning electron microscope (S-4800 Field-Emission Scanning Electron Microscope; Hitachi), and corrosion products were identified using an X-ray diffractometer (Rigaku D/MAX 2400) using Cu Kα radiation at a scan rate of 4°/min operated at 40 kV and 100 mA after immersion for 10, 42, and 120 days.

2.4. Electrochemical tests

Electrochemical tests were performed with a traditional three-electrode cell, with the control or treated samples as the working electrode, a saturated calomel electrode (SCE) as the reference electrode, and a platinum plate electrode as the counter electrode. Electrochemical tests were carried out in SUF. The exposure area of the specimen was 0.2826 cm^2. Variations in the free corrosion potential were monitored as a function of time under open circuit potential (OCP) conditions for approximately 1 h. Then potentiodynamic polarization was performed at a scanning rate of 1 mV/s. Corrosion parameters including OCP, corrosion potential (E_{corr}), and corrosion current density (i_{corr}) were estimated from the polarization curves by Tafel analysis based on the polarization plots. The Tafel slope was carefully determined in the potential range of 130–

Table 1
Ion concentrations in simulated uterine fluid (SUF) and other simulated body fluids or cell culture medium.

Body fluids	Na^+ (mmol/L)	K^+ (mmol/L)	Ca^+ (mmol/L)	Mg^{2+} (mmol/L)	Cl^- (mmol/L)	HCO_3^- (mmol/L)	$H_2PO_4^-$ (mmol/L)	HPO_4^{2-} (mmol/L)	SO_4^{2-} (mmol/L)	Glucose (g/L)	Amino acids (mg/L)	Reference
SUF	88.5	3.0	1.5	–	91.0	3.0	0.5	–	–	0.5	–	[59]
Plasma	142.0	5.0	2.5	1.5	103.0	27.0	–	1.0	0.5	–	–	[43]
SBF	142.0	5.0	2.5	1.5	148.5	4.2	–	1.0	0.5	–	–	[60]
m-SBF	142.0	5.0	2.5	1.5	103.0	10.0	–	1.0	0.5	–	–	[61]
Hank's	145.0	5.8	1.3	0.4	144.6	26.2	–	0.8	0.4	5.5	–	[43]
Earle(+)	151.0	5.4	1.8	0.8	125.0	26.2	0.9	–	0.8	1.0	0.9	[42]
E-MEM	151.0	5.4	1.8	0.8	125.0	26.2	0.9	–	0.8	1.1	0.9	[42]
DMEM	154.9	5.3	1.8	0.8	118.9	44.0	0.9	–	0.8	25	0.9	[62]

300 mV vs. SCE away from E_{corr} both on the cathodic curve and on the anodic curve, as the selection may cause large variations. Each test was conducted five times.

2.5. In vitro studies

2.5.1. Immunofluorescence assay

Human vascular smooth muscle cells (HVSMC) and three types of human uterine cells, namely, HUSMC, HEEC, and HESC, were adopted for the experiments. They were obtained from Shenzhen Procell Company, China. Some cells were fixed in cold ethanol/acetone (1:1, v/v) for 15 min and then washed with phosphate-buffered saline (PBS) 3 times, 5 min/wash. The cells were then incubated with 2% Triton X-100 for 5 min at room temperature for penetration. The cells were pretreated with 3% bovine serum albumin (BSA) before incubation with monoclonal anti-α-smooth muscle actin (1:300), anti-cytokeratin actin, or anti-vimentin actin antibody and incubated overnight at 4 °C. The cells were then washed 3 times with PBS, 5 min/wash and then incubated with secondary antibody in PBS with Tween 20 (PBST) in dark for 2 h at room temperature. The sections were mounted with an anti-fading mounting medium and visualized under a fluorescence microscope. Specificity of all the cells was found to be appropriate, as shown in Fig. S2.

2.5.2. CCK8 assay

All experimental cell lines were cultured in Dulbecco's Modified Eagle Medium (DMEM) or Dulbecco's Modified Eagle Medium: Nutrient Mixture F-12 (DMEM/F12; VSMC and HUSMC were cultured in DMEM, while HEEC and HESC were cultured in DMEM/F12) supplemented with 10% fetal bovine serum (FBS), 100 U•mL^{-1} penicillin, and 100 g•mL^{-1} streptomycin in a humidified atmosphere with 5% CO_2 at 37 °C. Polished samples were washed, air-dried, and sterilized by ultraviolet radiation for at least 4 h. Four kinds of extracts were prepared by incubating the samples in DMEM and DMEM/F12 supplemented with 10% FBS for 24 h at an extraction ratio of 1.25 cm^2/mL under standard cell culture conditions. The supernatant fluid was withdrawn and stored at 4 °C before use. The pH values of the extracts were measured using a pH meter (PB-10, Sartorius). Ion concentration in the extracts was determined using an inductively coupled plasma optical emission spectroscope (ICP-OES, iCAP6300, Thermo Scientific). The conventional medium was used as the negative control, and the culture medium added with 10% dimethylsulfoxide (DMSO) was adopted as the positive control.

Cell suspension (100 μL) was seeded in 96-well plates at a seeding density of 1×10^4 cells, and the cells were incubated for 24 h to allow attachment. Afterwards, the normal culture medium was replaced with 100% extract. To prevent interference, on 1, 3, and 5 days before the test, the extracts were replaced with normal culture medium. The cell viability was detected using Cell Counting Kit-8 (CCK-8, Dojindo Molecular Technologies, Japan). Each well of the plate was added with 10 μL of CCK-8 solution and subsequently incubated for 1 h in the incubator. The spectrophotometric absorbance of each well was measured with a microplate reader (Bio-Rad 680) at a single wavelength of 450 nm. Each test was performed five times.

2.6. In vivo studies

2.6.1. Animal treatment

Sexually mature female Sprague Dawley rats (weight range, 190–220 g, age, 8–9 weeks) were obtained from Charles River Laboratories, China. The animals were allowed to acclimatize for 1 week before carrying out the experiment and were bred under standard conditions. Drinking water and conventional feed were provided ad libitum. All protocols for animal care and treatment were approved by the Ethical Committee of National Research Institute for Family Planning. Thirty-six sexually mature female Sprague Dawley rats were randomly divided into four groups depending on the implanted materials, namely, the non-operation group (control group), the HP-Mg group, the Mg-1Ca group, and Mg-2Zn group, with nine rats in each group. Materials in the different groups were cut as a pin with 2 mm diameter and 2 mm thickness for use. To evaluate the possibility of future application as a fixing device for IUD, materials were implanted in the gluteal muscle of rats to measure the response of the muscle tissue. The animals in the HP-Mg, Mg-1Ca, and Mg-2Zn groups were anesthetized, and the corresponding material was implanted into the gluteus maximus muscle.

2.6.2. Histological analysis

The muscle tissues were collected on days 3, 10, and 28 after implantation. Muscle tissue samples were cut into 4×3 mm^2 pieces and fixed immediately in 4% (w/v) paraformaldehyde (pH 7.2) and incubated overnight at 4 °C; they were then transferred to a graded series of ethanol (70%, 75%, 80%, 95% I and II, and 100% I and II) and immersed in xylene and paraffin. Before hematoxylin and eosin (H&E) staining, 5-μm-thick muscle tissue sections were dewaxed in xylene, rehydrated with decreasing concentrations of ethanol (100% I and II, 95% I and II, 80%, 75%, 70%), and washed in PBS. Then they were stained with H&E. After staining, sections were dehydrated through increasing concentrations of ethanol (75%, 95% I and II, and 100% I and II) and xylene.

2.7. Statistical analysis

All repeated measurements data were presented as mean ± standard deviation (SD). Statistical significance of data was estimated through one-way analysis of variance (ANOVA) for multiple comparisons, and non-paired Student's t test was used

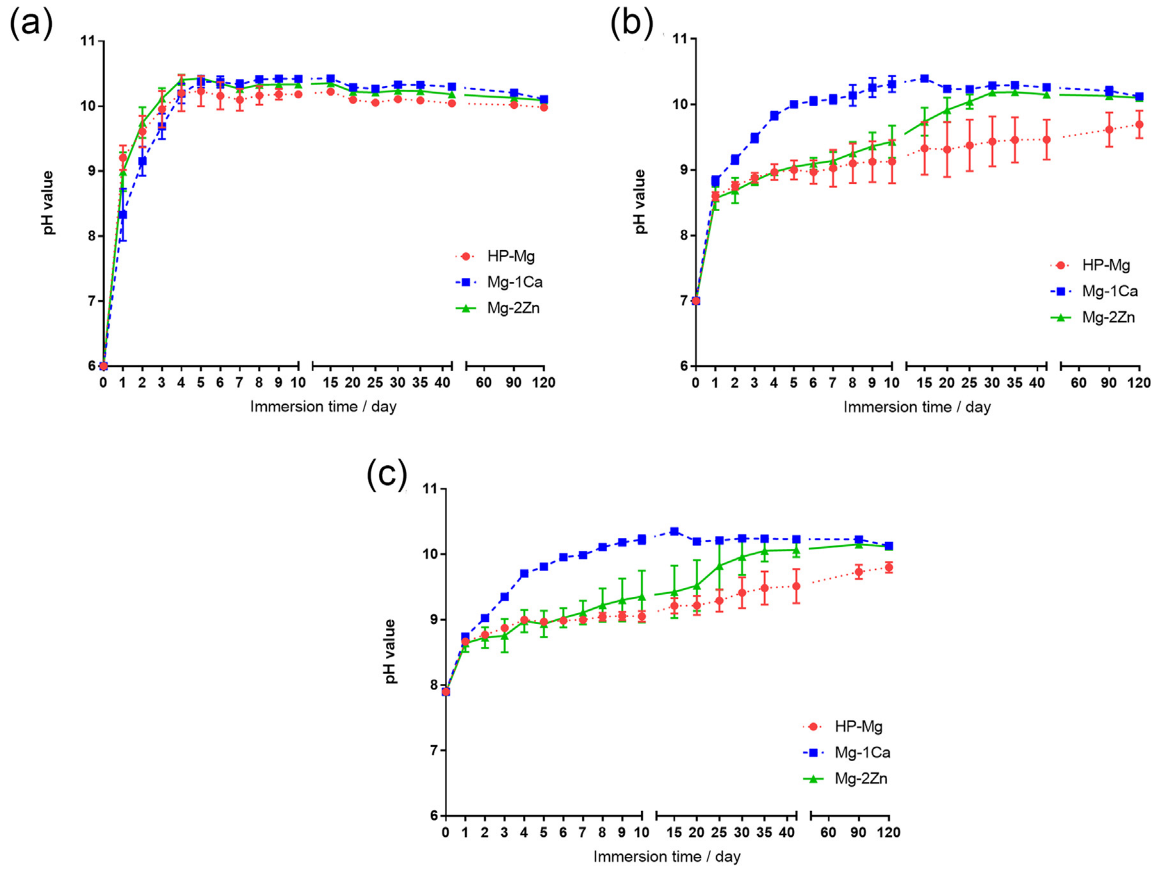

Fig. 1. Variation in pH values during immersion testing of HP-Mg, Mg-1Ca alloy, and Mg-2Zn alloy in SUF with preseted pH values of (a) 6.0, (b) 7.0, and (c) 7.9.

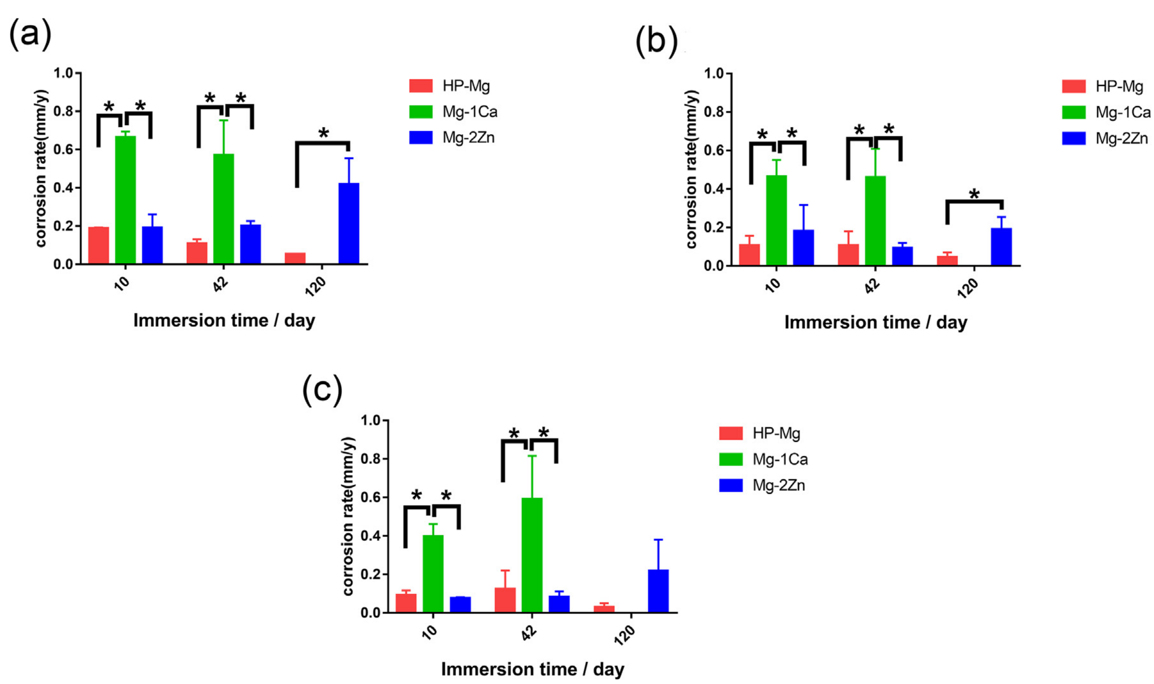

Fig. 2. Corrosion rates calculated from the weight loss of samples after static immersion for 10, 42, and 120 days in simulated uterine fluid with preseted pH values of (a) 6.0, (b) 7.0, and (c) 7.9.

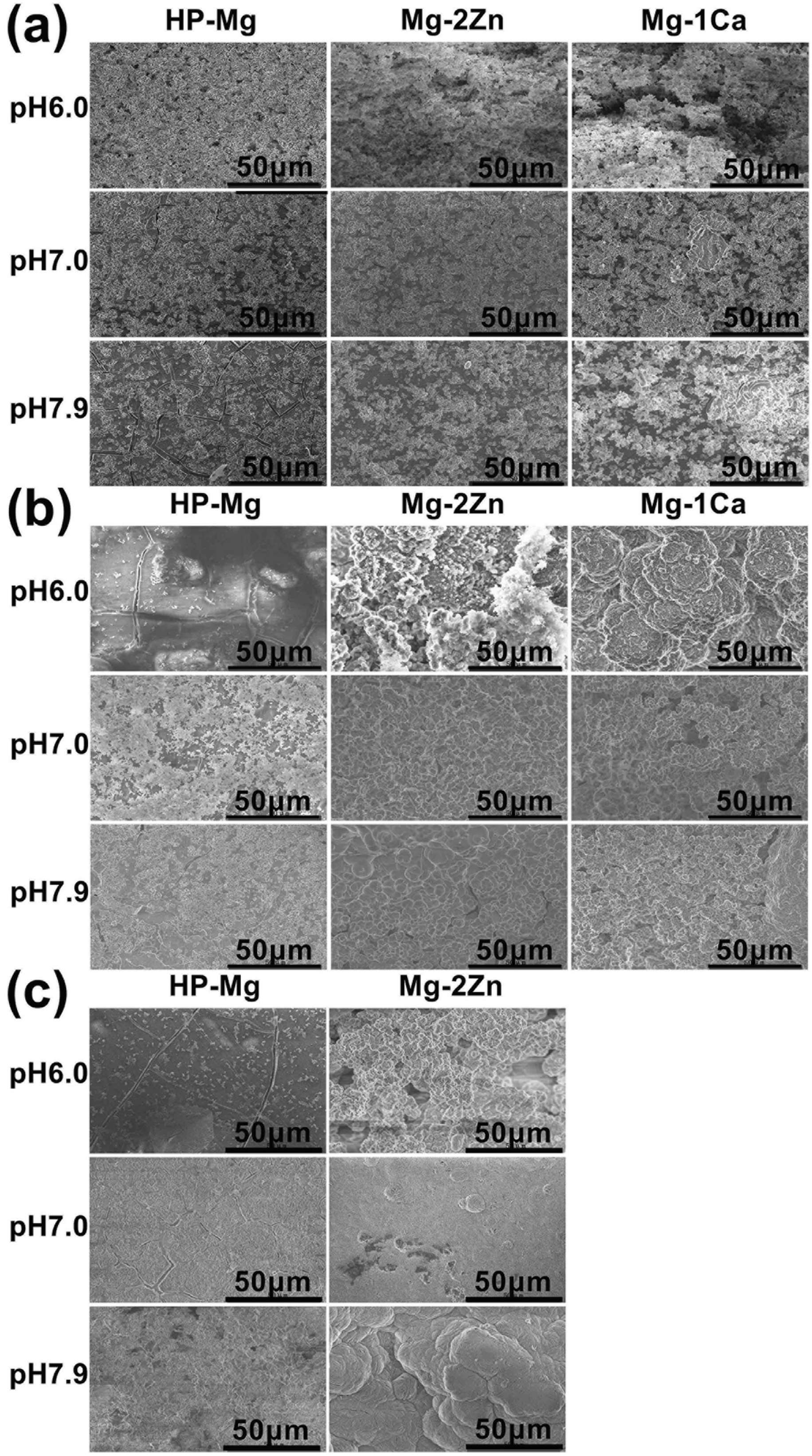

Fig. 3. SEM images of HP-Mg, Mg-1Ca alloy, and Mg-2Zn alloy immersed in SUF with preseted pH values of 6.0, 7.0, and 7.9 at different time points (a) 10 days, (b) 42 days, and (c) 120 days.

to compare two groups. Unless otherwise mentioned, the limit value of significance was set as p-value = 0.05 in all instances.

3. Results

3.1. Immersion tests

Fig. 1 presents the variation of measured pH values of SUF during the immersion period for different experimental material groups. As shown in Fig. 1(a), in the preseted pH = 6.0 group, the pH value of SUF increased rapidly to 10.5 after the first 4 days and then became stable. Compared with the preseted pH = 6.0 group, the preseted pH = 7.0 and preseted pH = 7.9 groups exhibited much longer time to reach a stable pH value, Mg-1Ca alloy took approximately 10 days, and Mg-2Zn alloy took approximately 30 to 35 days. In addition, the pH value of the HP-Mg in the preseted pH = 7.0 and preseted pH = 7.9 groups increased rapidly on the first day but later increased slowly during the whole immersion period.

Fig. 2 shows the average corrosion rate data at different time points calculated from the immersion tests. It showed the same tendency as the variation in pH value that the corrosion rate of Mg-1Ca alloy was significantly faster than those of HP-Mg and Mg-2Zn alloy, and the corrosion rate of Mg-2Zn alloy was higher than that of HP-Mg; these variation trends would weaken with the increase in the pH value of the SUF solution. Surface morphologies were observed using a three-dimensional microscope for HP-Mg, Mg-1Ca, and Mg-2Zn alloys exposed to the SUF solution after 10, 42, and 120 days of immersion as shown in Fig. S2, and the findings were in good agreement with the results of the corrosion rate test. After 10 days of immersion, in the three preseted pH groups, more white corrosion products formed on the surface of the Mg-1Ca alloy, and such products appeared to accumulate until they covered the entire surface up to day 42. In contrast, on the surface of HP-Mg, corrosion occurred at a random location throughout the entire 120 days of immersion, and white corrosion products could be seen on it. The extent of corrosion of the Mg-2Zn alloy was placed in between those of HP-Mg and Mg-1Ca alloy.

3.2. Surface characterization

The change in surface morphologies, observed by SEM, of HP-Mg, Mg-1Ca, and Mg-2Zn alloy samples throughout 120 days of immersion in the SUF of preseted values = 6.0, 7.0, and 7.9 is shown in Fig. 3. After immersion in SUF for 10 days, more corrosion products (a layer of loose corrosion products) were formed on the surface of Mg-1Ca alloy than on the surface of HP-Mg and Mg-2Zn alloys. Among the samples with three preseted pH values, less cor-

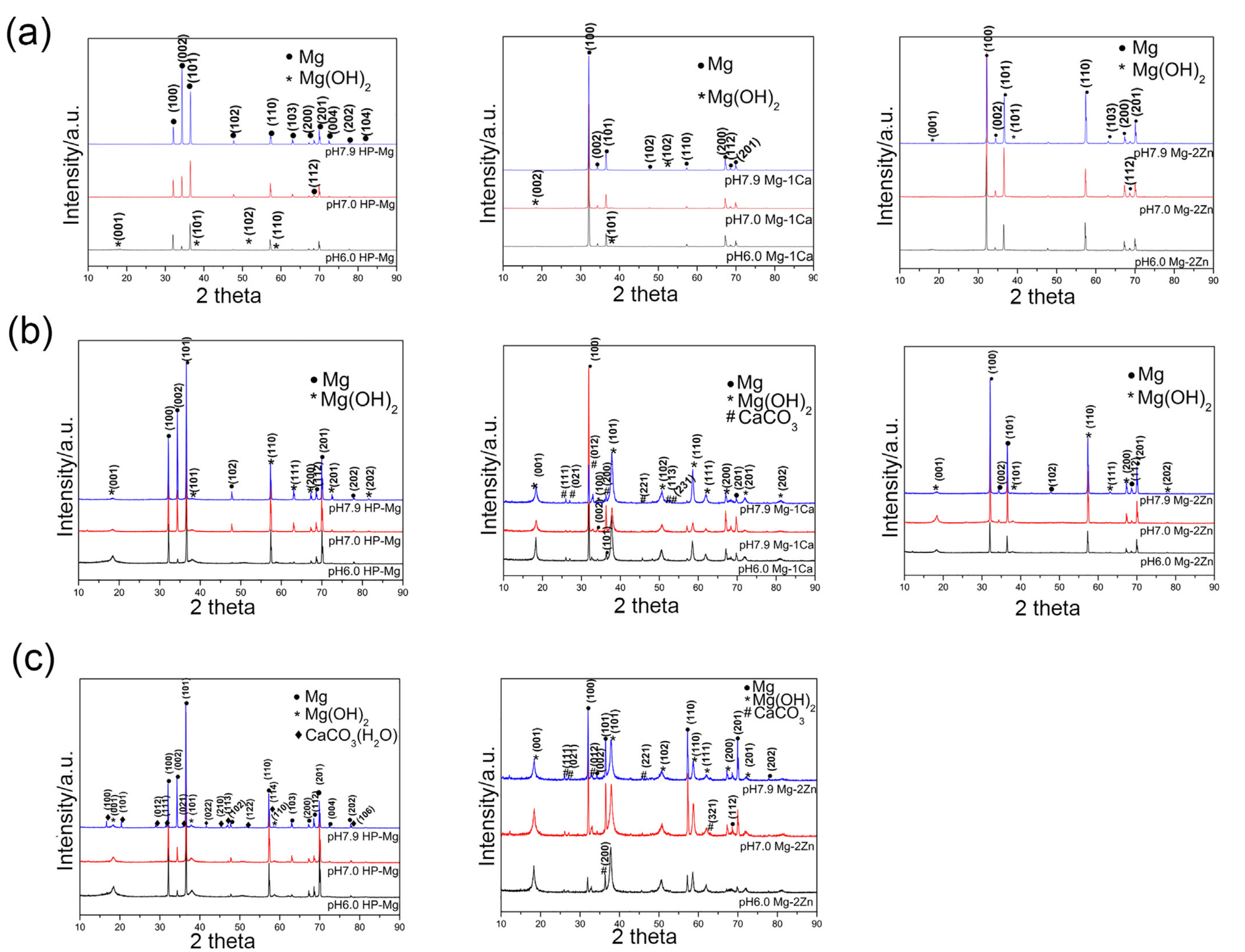

Fig. 4. XRD patterns of HP-Mg, Mg-1Ca alloy, and Mg-2Zn alloy immersed in SUF with preseted pH values of 6.0, 7.0, and 7.9 at different time points (a) 10 days, (b) 42 days, and (c) 120 days.

rosion products were formed on the surface of the preseted pH = 7.9 sample than on the surface of the other two preseted pH groups, and the original metal surface could be seen clearly. With the increase in immersion time, the corrosion product layer gradually thickened, and Mg-1Ca and Mg-2Zn alloys formed a dense corrosion product layer on the surface at 42 days. After 90 days of immersion, the Mg-1Ca alloy bulk disc sample was segmented into powder, and at 120 days, it completely dissolved in the SUF. HP-Mg and Mg-2Zn alloy samples remained there after 120 days of immersion, but more corrosion products formed on the surface of the Mg-2Zn alloy sample, whereas the least corrosion products formed on the surface of the HP-Mg sample. The chemical composition of corrosion products for the three experimental materials were detected by EDS mapping analysis at different time points; the results showed that the products were mainly composed of the elements Mg, Ca, C, O, and P as illustrated in Fig. S3.

Fig. 4(a)–(c) shows XRD patterns of HP-Mg, Mg-1Ca, and Mg-2Zn alloy samples immersed in the SUF for 10, 42, and 120 days. Based on XRD results, after immersion in the SUF for 10 days, the surface corrosion product on HP-Mg, Mg-1Ca, and Mg-2Zn alloy samples was mainly composed of $Mg(OH)_2$. On day 42 after immersion in the SUF, in addition to $Mg(OH)_2$, $CaCO_3$ was detected as new corrosion products on the Mg-1Ca alloy surface. With the increase in soaking time, in addition to $Mg(OH)_2$, $CaCO_3$ was identified on the Mg-2Zn alloy surface, whereas $CaCO_3{\cdot}H_2O$ was formed on the surface of HP-Mg.

3.3. Electrochemical measurements

Fig. 5 depicts the potentiodynamic polarization curves of various experimental materials in the SUF solution. The results of corrosion potentials (E_{corr}), corrosion current densities (i_{corr}), and corrosion rates, determined by the Tafel extrapolation method, are listed in Table 2. As expected, Mg-1Ca alloy showed the highest corrosion current density among the three material groups and exhibited the fastest corrosion rate in the preseted pH = 6.0 and pH = 7.9 groups.

3.4. In vitro cytocompatibility studies

Fig. 6 displays the cell viabilities in extract media of the HP-Mg, Mg-1Ca, and Mg-2Zn alloy samples. The effects of material composition on cell viabilities were found to be similar. Except for the

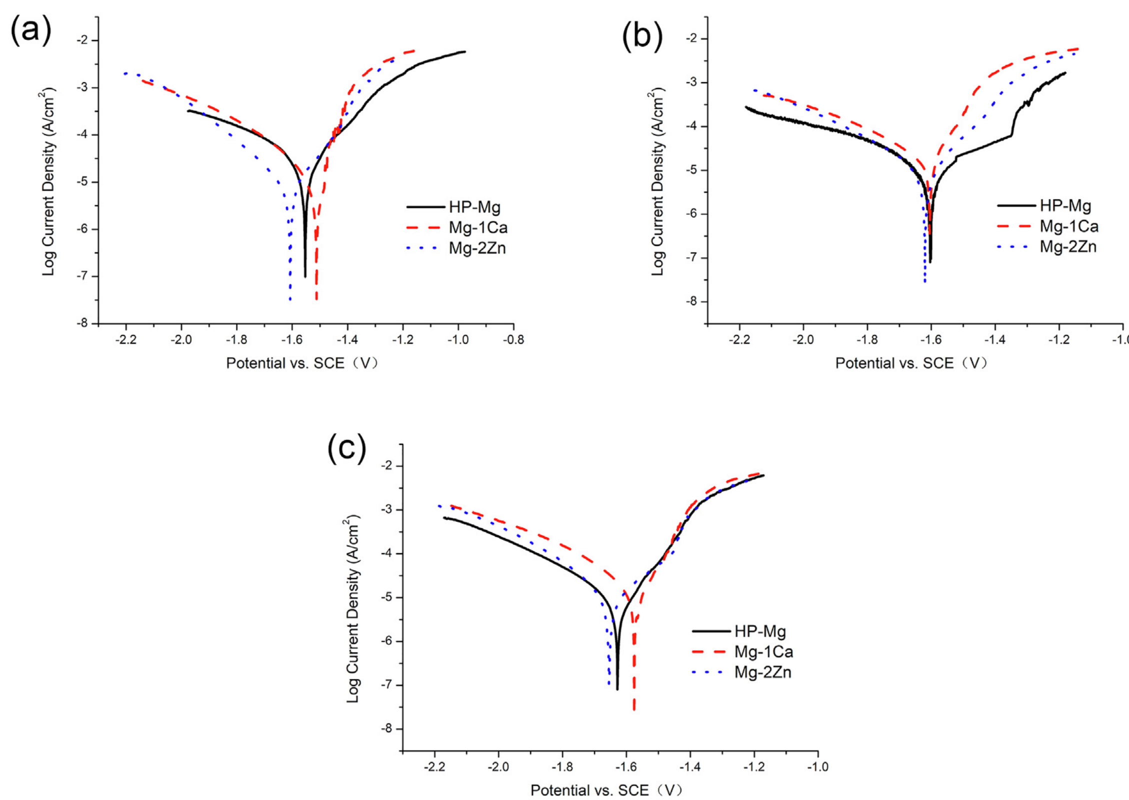

Fig. 5. Potentiodynamic polarization curves of HP-Mg, Mg-1Ca alloy, and Mg-2Zn alloy in SUF with preseted pH values of (a) 6.0, (b) 7.0, and (c) 7.9.

Table 2
Parameters E_{corr} and i_{corr} and corrosion rates of HP-Mg, Mg-1Ca alloy, and Mg-2Zn alloy in SUF with (a) preseted pH = 6.0, (b) preseted pH = 7.0, and (c) preseted pH = 7.9.

pH value	6.0			7.0			7.9		
Material	E_{corr}/V vs. SCE	i_{corr} A/cm^2	Corrosion rate mm/year	E_{corr}/V vs. SCE	i_{corr} A/cm^2	Corrosion rate mm/year	E_{corr}/V vs. SCE	i_{corr} A/cm^2	Corrosion rate mm/year
HP-Mg	−1.54 ± 0.01	$1.76 \pm 0.01 \times 10^{-5b}$	0.80 ± 0.01^{b}	−1.59 ± 0.04	$1.35 \pm 0.38 \times 10^{-6}$	0.62 ± 0.17	-1.59 ± 0.02^{b}	$1.42 \pm 0.62 \times 10^{-5a}$	0.65 ± 0.28^{a}
Mg-1Ca	−1.59 ± 0.01	$2.87 \pm 0.30 \times 10^{-5c}$	1.33 ± 0.12^{c}	−1.58 ± 0.01	$1.29 \pm 0.13 \times 10^{-5}$	0.59 ± 0.06	-1.56 ± 0.01^{a}	$1.69 \pm 0.21 \times 10^{-5b}$	0.78 ± 0.10^{b}
Mg-2Zn	−1.57 ± 0.02	$5.61 \pm 1.07 \times 10^{-6a}$	0.27 ± 0.05^{a}	−1.64 ± 0.02	$1.10 \pm 0.20 \times 10^{-5}$	0.53 ± 0.10	-1.64 ± 0.01^{c}	$1.13 \pm 0.09 \times 10^{-5a}$	0.55 ± 0.04^{a}

Different letters (a, b, c) mean statistically significant difference between HP-Mg, Mg-1Ca, and Mg-2Zn alloys.

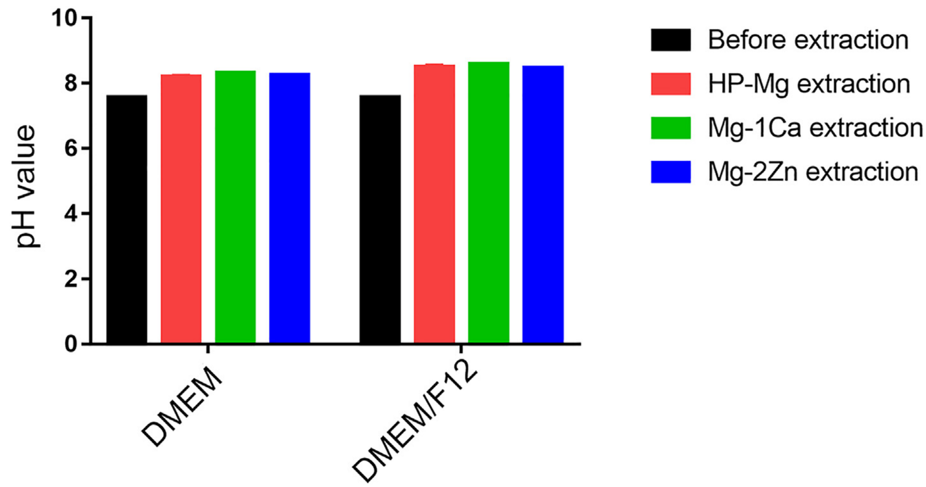

Fig. 6. **V**iability of (a) HVSMCs, (b) HUSMCs, (c) HEECs, and (d) HESCs after 1, 3, and 5 days of incubation of HP-Mg, Mg-1Ca alloy, and Mg-2Zn alloy extracts, normal medium, and normal (negative control) with 10% DMSO (positive control).

HUSMC, the viabilities of other three kinds of cells increased in three days and decreased slightly in five days. As for HUSMC, the cell viability decreased slightly in three days and increased significantly in five days.

The cell cycle growth states, along with proliferation index after culturing in extracts of HP-Mg, Mg-1Ca alloy, and Mg-2Zn alloy, are listed in Table 3. Compared to the control, the S phase of HESC exposed to HP-Mg, Mg-1Ca, and Mg-2Zn alloy extracts possessed high percentage, and among them, the Mg-1Ca alloy group has a statistically significant level and higher proliferation index (PI).

Fig. 7 presents the pH values of the extract media. Because of the presence of the agent in DMEM and DMEM/F12, there is no sig-

Table 3
Cell cycle and proliferation index (PI) of HESC exposed to culture media (mean ± SD). # Proliferation index (PI) represents the ratio of between the S phase and the G2/M phase in the whole cell cycle (i.e., PI = (S + G2/M) / (G0 / G1 + S + G2/M), cell proliferation ratio = PI × 100%).

Groups	G0/G1 (%)	S (%)	G2/M (%)	PI (%)#
NC	69.1 ± 0.65	18.66 ± 0.41	12.25 ± 0.26	30.91 ± 0.65
HP-Mg	64.42 ± 0.49	19.23 ± 0.86	16.36 ± 0.37	35.59 ± 0.49**
Mg-1Ca	64.47 ± 0.83	19.78 ± 0.18*	15.76 ± 1.01	35.53 ± 0.83**
Mg-2Zn	64.54 ± 0.35	19.61 ± 0.21	15.87 ± 0.13	35.47 ± 0.34**

*Statistically significant difference between HP-Mg, Mg-1Ca alloy, Mg-2Zn alloy, and MEM Control, * $p < 0.05$, ** $p < 0.01$

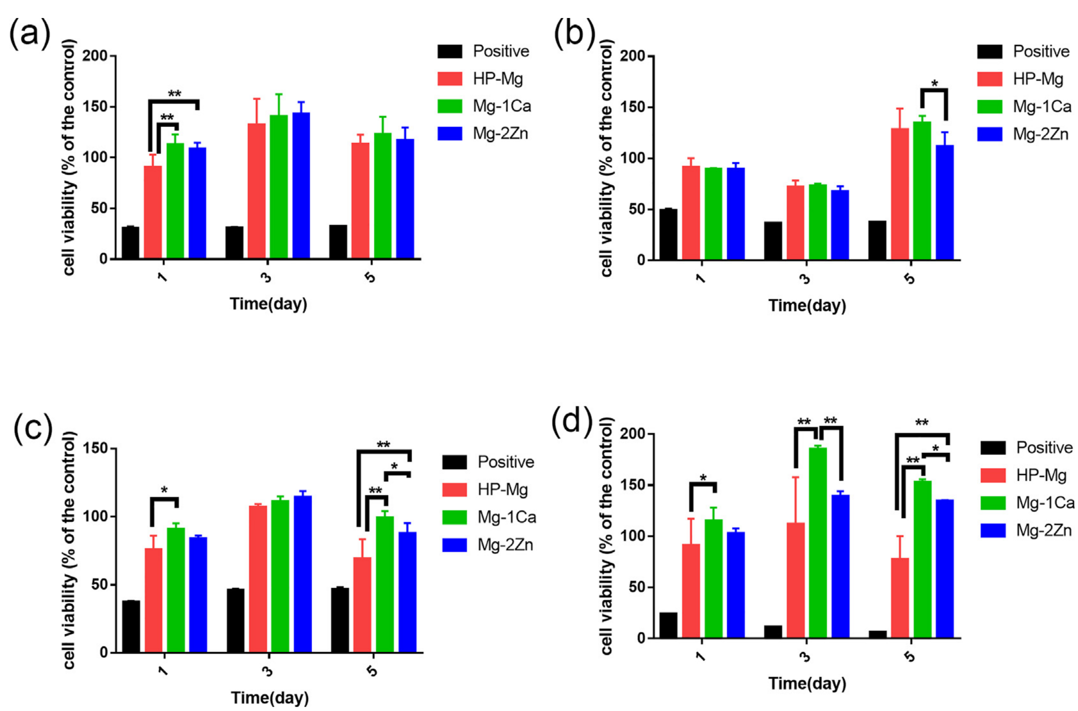

Fig. 7. pH values of the DMEM and DMEM/F12 before and after adding the extract.

nificant difference in the pH values among the three kinds of extracts.

Table 4 shows the ion concentration in HP-Mg, Mg-1Ca alloy, and Mg-2Zn alloy extracts. The concentrations of Mg^{2+} in the extracts of the four cell culture media were ranked as HP-Mg > Mg-1Ca > Mg-2Zn. Moreover, it is apparent that the Mg^{2+} content of the HP-Mg group extract in the culture medium of HESC was highest.

To investigate the inflammatory response, we studied the IL-1β, IL-6, IL-8, and TNF-α expression, representative of pro-inflammatory cytokines. Fig. 8 shows the IL-1β, IL-6, IL-8, and TNF-α expression in HESC treated with HP-Mg, Mg-1Ca alloy, and Mg-2Zn alloy extracts. Compared with the control group, IL-1β and IL-6 expression in HP-Mg and Mg-1Ca alloy groups was significantly decreased ($p < 0.05$). IL-8 expression in the HP-Mg group was lower than that in the control group ($p < 0.05$), while IL-8 expression in the Mg-2Zn alloy group was higher than that in the control group ($p < 0.05$). Additionally, TNF-α expression in the HP-Mg group was significantly decreased compared with that in the control group ($p < 0.05$).

Table 4
Ion concentration of HP-Mg, Mg-1Ca alloy, and Mg-2Zn alloy immersed in four culture media for 24 h.

	Mg (mM)			Ca (mM)	Zn (mM)
	HP-Mg	Mg-1Ca	Mg-2Zn	Mg-1Ca	Mg-2Zn
VSMC	4.59	4.61	3.85	1.24	0.005
HUSMC	3.62	3.19	2.73	1.28	0.005
HEEC	3.85	3.42	3.29	1.26	0.002
HESC	37.75	28.21	7.44	0.69	0.011
	Mg(mM)		Ca(mM)		Zn(mM)
VSMC	0.74		1.30		0.004
HUSMC	0.76		1.46		0.004
HEEC	0.75		1.28		0.001
HESC	0.71		1.32		0.009

3.5. In vivo animal experiment

To evaluate the tissue response to the implant, the gluteus maximus muscle of rat was used as the implantation position. Fig. 9 shows the histological images of the tissues around the HP-Mg, Mg-1Ca alloy, and Mg-2Zn alloy implants after 3, 10, and 28 days of implantation. For the control group, there is no inflammation reaction in the muscle tissue at the three time points. In contrast, an obvious connective tissue was formed around the HP-Mg implant, and a distinct cavity (indicated by triangle) can be observed at low magnification. The connective tissue layer formed on the implanted HP-Mg, Mg-1Ca alloy, and Mg-2Zn alloy sample surfaces was more pronounced as the implantation time increases. Furthermore, the inflammatory response gradually reduced. In the first 3 days, it was mainly an acute inflammatory reaction, and the nucleus of neutrophils could be significantly observed for all the three experimental materials (indicated by arrows). The inflammatory reaction was the least for the HP-Mg group, followed by the Mg-1Ca alloy group and the Mg-2Zn alloy group. After 28 days of implantation, it could be seen that the implants were surrounded mainly by connective tissue and lymphocytes were rarely observed. To study the effects of metal ion release on the muscle tissue, we observed the reaction of connective tissue and muscle layer and found that implants had little effect on muscle tissue.

4. Discussion

4.1. Comparison of degradation products in SUF with those in other simulated body fluids

Several in vitro studies have revealed the corrosion products of HP Mg, Mg-Ca alloy, and Mg-Zn alloy after immersion in various simulated body solutions as listed in Table 5. Generally, it was recognized that the initial oxidation of Mg proceeds through three steps: (1) oxygen chemisorption, (2) formation of the oxide layer,

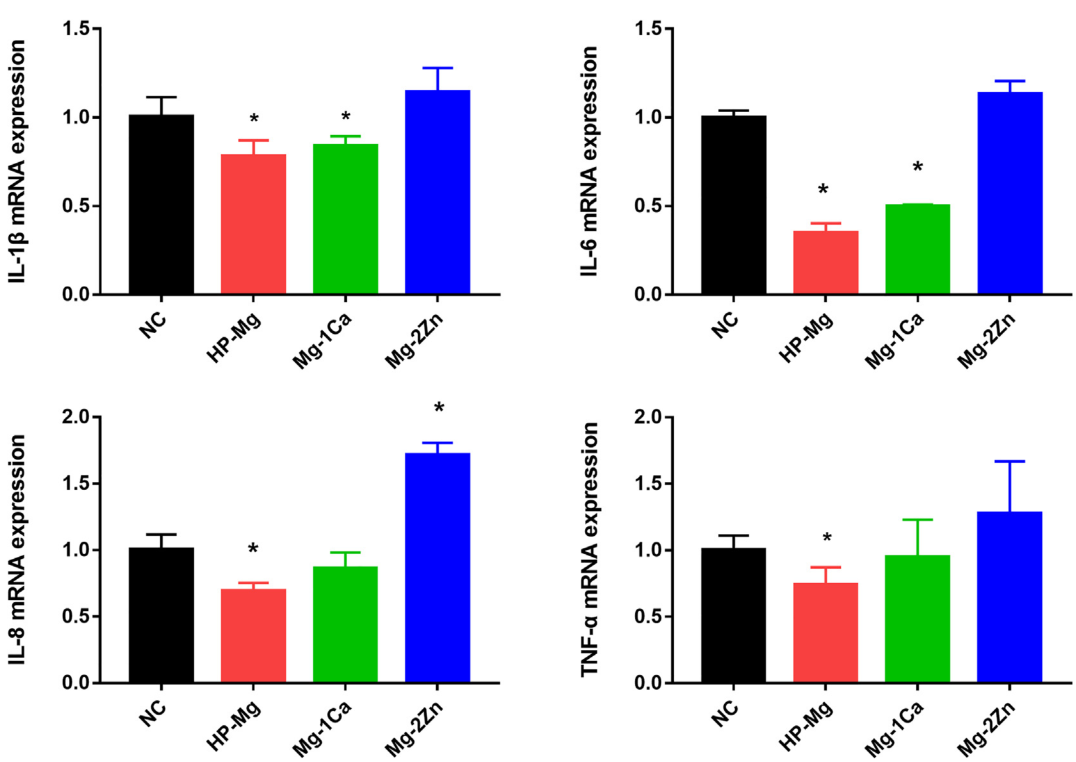

Fig. 8. IL-1β, IL-6, IL-8, IFN-γ, and TNF-α expression in HESCs in HP-Mg, Mg-1Ca alloy, and Mg-2Zn alloy extract media.

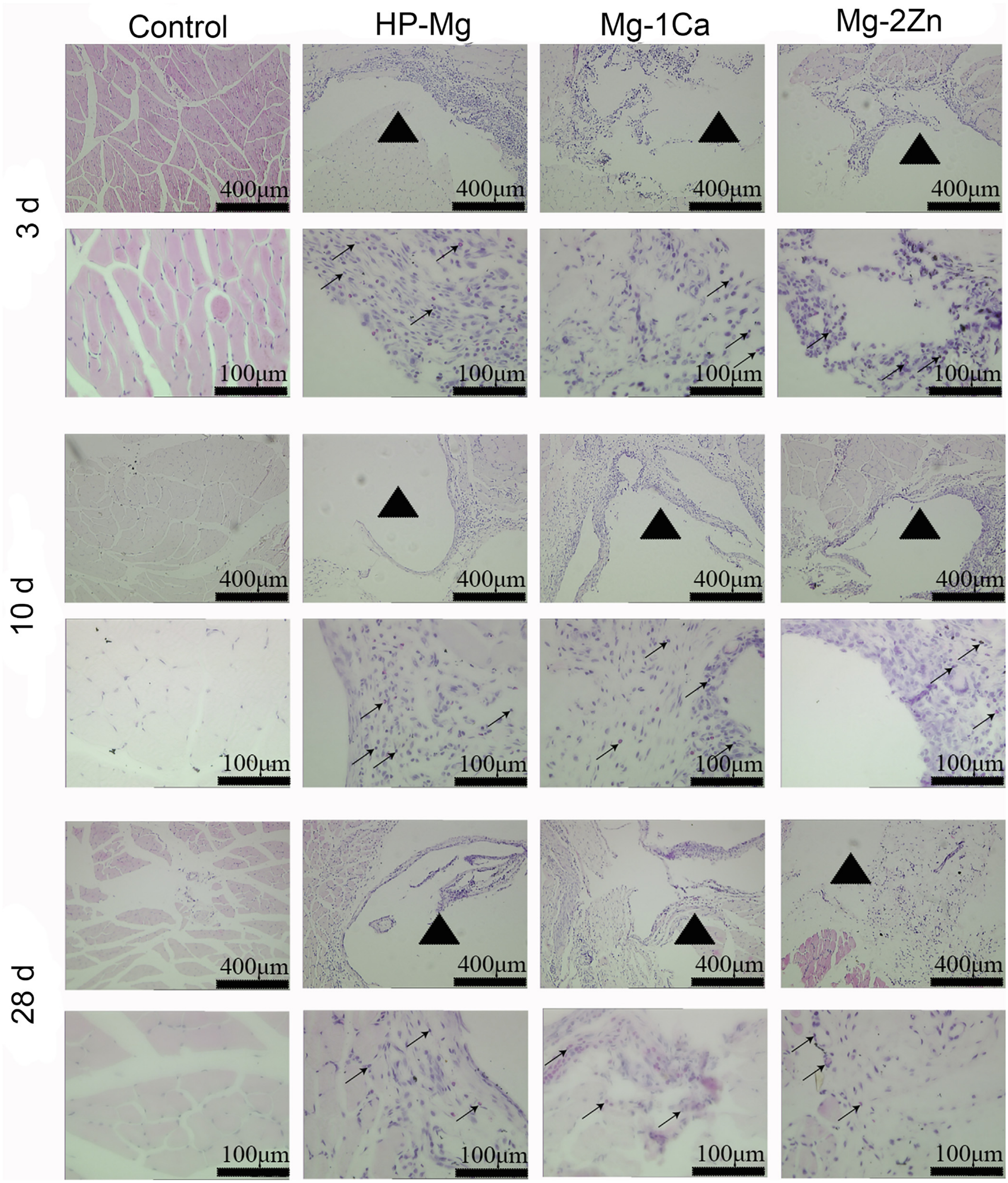

Fig. 9. Histological photographs of hematoxylin-eosin staining of Sprague Dawley rat muscle with HP-Mg, Mg-1Ca alloy, and Mg-2Zn alloy after implantation for A (3 d), B (10 d), and C (28 d).

and (3) oxide thickening. In general, the $Mg(OH)_2$ phase was the main product on the surface of the previously reported Mg alloys [22,33,38–41]. In this study, $Mg(OH)_2$ was first formed due to the biodegradation of HP-Mg, Mg-1Ca, and Mg-2Zn alloys in the SUF, which is similar to that reported in the NaCl solution [42] and Hank's solution added with HEPES buffer [43]. $CaCO_3{\cdot}H_2O$ was detected as the corrosion products of HP-Mg and $CaCO_3$ was detected in the corrosion products of Mg-1Ca and Mg-2Zn alloys after immersing in the SUF for 42 days and 120 days, respectively. First, Ca was first soluble in the magnesium matrix, and then, a second Mg_2Ca phase could be identified in the Mg-1Ca alloy [33]. When the magnesium matrix first corrodes, Ca is released in the form of ions into the solution. Second, when the Mg matrix corrodes to a certain extent, the second phase will also peel into the solution to undergo corrosion; this process also releases Ca ions into the solution. In addition, a study of the characterization of calcified deposits on IUD indicated that the rate of $CaCO_3$ formation depended not only on the size and quality of the IUD but also on the individual capability of the uterus to produce calcium ions [44]. Compared with the HP-Mg and Mg-2Zn alloy, the composition of calcium in the Mg-1Ca alloy may be the reason for the formation of $CaCO_3$ after immersion for 42 days. In a previous work, $CaCO_3$ or $MgCO_3$ and Ca/P were found in Hank's solution added with $NaHCO_3/CO_2$ buffer [43], in which CO_2 or $NaHCO_3$ reacted with $Mg(OH)_2$ and formed carbonates. Clearly, different chemical compositions of the tissue would result in different chemical reactions, forming different corrosion products. For example, in human bile, $Mg(H_2PO_4)_2$ was formed on the HP-Mg surface and increased the corrosion resistance [45]. In addition, in the artificial saliva, complex Ca/P products (OCP, DCPD, TCP) were detected [12]. In artificial urine, EDS results showed that Mg, O, P, Ca, and Na were present on the corrosion surface [10]. In the present work, $CaCO_3\cdot H_2O$ appeared in the corrosion products of HP-Mg after immersion for 120 days, which is likely due to the pH value and the ratio of Mg^{2+}/Ca^{2+} in the solution [46].

4.2. Feasibility of Mg alloys used in intrauterine microenvironment and proposed medical device

The uterus is an inverted pear-shaped, hollow, thick-walled fibromuscular female reproductive organ. Biomaterial-based products should meet certain requirements to be compatible with specific physiological and pathological processes of the uterus. As recommended by the World Health Organization (WHO) for postpartum family planning (PPFP) programs, IUD is a safe, convenient, and effective option for postpartum contraception [47]. However, the fall out of IUD, which occurs when immediately inserted after cesarean, remains to be solved [48–50]. GyneFix® is a specially designed IUD that can be anchored into the myometrium using a PDLGA cone. It is the only IUD with an anchor. The biodegradable cone part is made of PDLGA, and it would degrade into lactic acid and water after 2–3 months [51]. However, its limitation is the strong hygroscopicity, low heat stability [52], and poor flexibility to elongate [53]. As the strength of the fixation part, which is made of polymers, is not strong enough, it has to be built into a large cone. Compared with traditional metal biomaterials, biodegradable magnesium and its alloys can be used as future biomaterials owing to their good biodegradability, higher strength than polymers, acceptable ductility, good machinability, and potential for preventing a reoperation after the implant has fulfilled its purpose in the human body [1]. The potential applications of magnesium alloys for obstetrics and gynecology are proposed as follows: (*i*) absorbable IUD fixation device, (*ii*) IUA treatment pad as mechanical

Table 5
Comparison of degradation products in the SUF with those in other simulated body fluids.

Materials	Composition	Medium	Corrosion products	Reference
HP Mg	99.99%	SUF	$Mg(OH)_2$ $CaCO_3\cdot H_2O$	In this paper
	99.99%	SBF	$Mg(OH)_2$ HA CO_3^{2+}	[63]
	99.99%	SBF	$Mg(OH)_2$ Ca/P	[54]
	99.98%	Hank's + HEPES Earle + HEPES MEM + HEPES	$Mg(OH)_2$	[43]
		Hank's + $NaCO_3/CO_2$	$Mg(OH)_2$ Ca/P CO_3^{2+}	
	99.95%	DMEM	$Mg(OH)_2$	[64]
	99.95%	Bile	$Mg(H_2PO_4)_2$	[22]
	99.9%	NaCl	$Mg(OH)_2$	[42]
		NaCl + $NaCO_3$	$MgCO_3$	
		NaCl + HEPES	$Mg(OH)_2$	
		Earle(+)	Ca/P	
		E-MEM	Ca/P	
Mg-Zn alloy	Mg-2Zn	SUF	$Mg(OH)_2$ $CaCO_3$	In this paper
	Mg-6Zn	SBF	$Mg(OH)_2$ HA	[65]
	Mg-1,3Zn	NaCl	$Mg(OH)_2$	[66]
	Mg-6Zn	Ring's SBF	$Mg(OH)_2$	[67]
	10%-$Ca(PO_4)$/Mg-6Zn	Ring's SBF	$Mg(OH)_2$ HA β-$Ca(PO_4)$	
	Mg-2Zn	DMEM	O Mg Zn Cl	[64]
Mg-Ca alloy	Mg-1Ca	SUF	$Mg(OH)_2$ $CaCO_3$	In this paper
	Mg-1,2,3Ca	SBF	$Mg(OH)_2$ HA	[33]
	Mg-1,5,10Ca	DMEM	$Mg(OH)_2$ HA $CaCO_3$ $MgCO_3\cdot 3H_2O$	[62]
	Mg-1Ca	Hank's	$Mg(OH)_2$ Ca/P	[15]

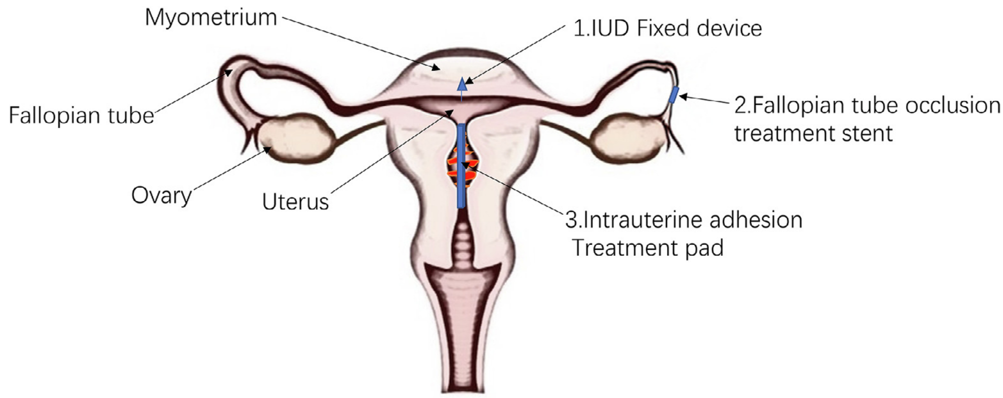

Fig. 10. Proposed future application of biomedical Mg alloys in obstetrics and gynecology.

barriers to separate traumatized tissues during the healing period and can reduce postoperative adhesions, and (*iii*) fallopian tube occlusion treatment stent, as shown in Fig. 10. The implantation positions for in vivo studies on devices used in obstetrics and gynecology, such as IUD fixation/anchoring part, IUA treatment pad, and fallopian tube occlusion treatment stent, are the uterus myometrium, uterine cavity, and fallopian tube, respectively. Future studies are expected to optimally design related medical devices based on the geometric size of the implantation position and the degradation rate of the magnesium alloys of interest and to test the feasibility with the correct animal models. Parallel comparative studies on existing materials or medical devices used in obstetrics and gynecology are also needed to prove the superiority with magnesium alloys.

The uterine tissue is composed by multiple kinds of cells, including HEEC, HESC, HUSMC, VSMC, and so on. In the present study, we examined the effects of the extract of experimental magnesium alloys on the cell proliferation and differentiation and found that the three kinds of experimental magnesium alloys have no cytotoxic effect on HEEC, HESC, HUSMC, and VSMC, as shown in Fig. 6, which is consistent with the results of previous studies [33,54]. Moreover, endometrial stromal cells play a key role in the periodic changes of the uterus and the process of placental implantation [55–57]; therefore, we have mainly observed the effects of the material on stromal cells. The expression of inflammatory factors, namely, IL-1β, IL-6, and IL-8 expression, in the HP-Mg and Mg-1Ca alloy groups is significantly lower than that in the control and Mg-2Zn alloy groups. TNF-α expression also demonstrated a similar trend. In previous studies, magnesium alloys were applied in orthopedic implants and showed the effect of promoting osteogenesis [33,58]. The human uterine wall is relatively special and has a very thick myometrium, but it is difficult to make an implantation in situ in other animals. Therefore, we used muscle tissues to replace the myometrium implantation in this paper. Three days after the implantation of magnesium and its alloys, an acute inflammatory response was observed around the implants (Fig. 9). The sequencing of the inflammatory response at the initial level was HP-Mg < Mg-1Ca < Mg-2Zn, which is similar to the reaction of inflammatory factors in cells. After 10 days of implantation, the fibrous connective tissue was wrapped around the implant, forming a wrapping layer with a slight chronic inflammatory reaction. Furthermore, after 28 days of implantation, the fibrous tissue layer on the implant surface was more pronounced. The results from H&E staining showed that there were very few inflammatory cells in the fibrous connective tissue in direct contact with the implant, indicating that magnesium and its alloys have good histocompatibility with the muscle tissue.

5. Conclusions

In this study, the biomedical Mg alloys HP-Mg, Mg-1Ca, and Mg-2Zn alloys were investigated for their feasibility to be used as uterine medical devices by in vitro and in vivo tests. The results indicate that the corrosion products of magnesium and its alloys immersed in the SUF were slightly different from those of magnesium and its alloys degraded within other microenvironments, and the results showed satisfactory in vitro and in vivo biocompatibility. The following conclusions could be drawn:

(1) $Mg(OH)_2$ could be formed as the main corrosion product during the degradation of HP-Mg, Mg-1Ca alloy, and Mg-2Zn alloy in the SUF. In addition, $CaCO_3$ and $CaCO_3{\cdot}H_2O$ were formed with longer immersion time.
(2) HP-Mg, Mg-1Ca alloy, and Mg-2Zn alloy showed no cytotoxic effect on the uterine cells (HUSMCs, HEECs, and HESCs) and VSMCs.
(3) In vivo experiment shows that HP-Mg, Mg-1Ca alloy, and Mg-2Zn alloy implants cause a slight inflammatory response in the initial 3 days, but they were surrounded mainly by connective tissue, and lymphocytes were rarely observed at 4 weeks.

Acknowledgments

This work was supported by the National Key R&D Program of China (Grant No. 2016YFC1000903), Central Public-Interest Scientific Institution Basal Research Fund (Grant No. 2016GJZ03), National Natural Science Foundation of China (Grant No. 51431002 and 51871004), NSFC/RGC Joint Research Scheme (Grant No. 51661165014), and Peking University Medicine Seed Fund for Interdisciplinary Research (Grant No. BMU2018ME005).

Appendix A. Supplementary data

Supplementary data to this article can be found online at https://doi.org/10.1016/j.actbio.2019.08.001.

References

[1] Y.F. Zheng, X.N. Gu, F. Witte, Biodegradable metals, Mater. Sci. Eng. R Rep. 77 (2014) 1–34.
[2] F. Witte, Reprint of: the history of biodegradable magnesium implants: a review, Acta Biomater. 23 (2015) S28–S40.

[3] F. Witte, The history of biodegradable magnesium implants: a review, Acta Biomater. 6 (2010) 1680–1692.
[4] C. Yu, L.Y. Cui, Y.F. Zhou, Z.Z. Han, X.B. Chen, R.C. Zeng, Y.H. Zou, S.Q. Li, F. Zhang, E.H. Han, S.K. Guan, Self-degradation of micro-arc oxidation/chitosan composite coating on Mg-4Li-1Ca alloy, Surf. Coat. Technol. 344 (2018) 1–11.
[5] Z. Fang, J. Wang, X. Yang, Q. Sun, Y. Jia, H. Liu, T. Xi, S. Guan, Adsorption of arginine, glycine and aspartic acid on Mg and Mg-based alloy surfaces: a first-principles study, Appl. Surf. Sci. 409 (2017) 149–155.
[6] L.Y. Li, L.Y. Cui, R.C. Zeng, S.Q. Li, X.B. Chen, Y. Zheng, M.B. Kannan, Advances in functionalized polymer coatings on biodegradable magnesium alloys-a review, Acta Biomater. 79 (2018) 23–36.
[7] R.C. Zeng, W.C. Qi, H.Z. Cui, F. Zhang, S.Q. Li, E.H. Han, In vitro corrosion of as-extruded Mg-Ca alloys-the influence of Ca concentration, Corros. Sci. 96 (2015) 23–31.
[8] Y. Xin, C. Liu, X. Zhang, G. Tang, X. Tian, P.K. Chu, Corrosion behavior of biomedical AZ91 magnesium alloy in simulated body fluids, J. Mater. Res. 22 (2011) 2004–2011.
[9] F. Witte, J. Fischer, J. Nellesen, H.A. Crostack, V. Kaese, A. Pisch, F. Beckmann, H. Windhagen, In vitro and in vivo corrosion measurements of magnesium alloys, Biomaterials 27 (2006) 1013–1018.
[10] R.C. Zeng, X.T. Li, L.J. Liu, S.Q. Li, F. Zhang, In vitro Degradation of Pure Mg for Esophageal Stent in Artificial Saliva, J. Mater. Sci. Technol. 32 (2016) 437–444.
[11] Y. Liu, S. Zheng, N. Li, H. Guo, Y. Zheng, J. Peng, Study on the in vitro degradation behavior of pure Mg and WE43 in human bile for 60 days for future usage in biliary, Mater. Lett. 179 (2016) 100–103.
[12] J.Y. Lock, E. Wyatt, S. Upadhyayula, A. Whall, V. Nuñez, V.I. Vullev, H. Liu, Degradation and antibacterial properties of magnesium alloys in artificial urine for potential resorbable ureteral stent applications, J. Biomed. Mater. Res. Part A 102 (2014) 781–792.
[13] J.M. Seitz, A. Lucas, M. Kirschner, Magnesium-Based Compression Screws: A Novelty in the Clinical Use of Implants, JOM 68 (2016) 1177–1182.
[14] H.M. Garcia-Garcia, M. Haude, K. Kuku, A. Hideo-Kajita, H. Ince, A. Abizaid, R. Tölg, P.A. Lemos, C. von Birgelen, E.H. Christiansen, W. Wijns, J. Escaned, J. Dijkstra, R. Waksman, In vivo serial invasive imaging of the second-generation drug-eluting absorbable metal scaffold (Magmaris—DREAMS 2G) in de novo coronary lesions: Insights from the BIOSOLVE-II First-In-Man Trial, Inter. J. Cardiol. 255 (2018) 22–28.
[15] Y. Liu, D. Bian, Y. Wu, N. Li, K. Qiu, Y. Zheng, Y. Han, Influence of biocompatible metal ions (Ag, Fe, Y) on the surface chemistry, corrosion behavior and cytocompatibility of Mg-1Ca alloy treated with MEVVA, Coll. Surf. B Biointerfaces 133 (2015) 99–107.
[16] C. Zhao, F. Pan, S. Zhao, H. Pan, K. Song, A. Tang, Microstructure, corrosion behavior and cytotoxicity of biodegradable Mg-Sn implant alloys prepared by sub-rapid solidification, Mater. Sci. Eng. C Mater. Biol. Appl. 54 (2015) 245–251.
[17] Z. Zhen, B. Luthringer, L. Yang, T. Xi, Y. Zheng, F. Feyerabend, R. Willumeit, C. Lai, Z. Ge, Proteomic profile of mouse fibroblasts exposed to pure magnesium extract, Mater. Sci. Eng: C 69 (2016) 522–531.
[18] J. Liu, Y. Zheng, Y. Bi, Y. Li, Y. Zheng, Improved cytocompatibility of Mg-1Ca alloy modified by Zn ion implantation and deposition, Mater. Lett. 205 (2017) 87–89.
[19] M.S. Song, R.C. Zeng, Y.F. Ding, R.W. Li, M. Easton, I. Cole, N. Birbilis, X.B. Chen, Recent advances in biodegradation controls over Mg alloys for bone fracture management: a review, J. Mater. Sci. Technol. 35 (2019) 535–544.
[20] L. Cui, L. Sun, R. Zeng, Y. Zheng, S. Li, In vitro degradation and biocompatibility of Mg-Li-Ca alloys—the influence of Li content, Sci. China Mater. 61 (2017) 607–618.
[21] J.C. King, The Risk of Maternal Nutritional Depletion and Poor Outcomes Increases in Early or Closely Spaced Pregnancies, J. Nutr. 133 (2003) 1732s–1736s.
[22] Y. Liu, Y. Wu, D. Bian, S. Gao, S. Leeflang, H. Guo, Y. Zheng, J. Zhou, Study on the Mg-Li-Zn ternary alloy system with improved mechanical properties, good degradation performance and different responses to cells, Acta Biomater. 62 (2017) 418–433.
[23] M. Bornapour, H. Mahjoubi, H. Vali, D. Shum-Tim, M. Cerruti, M. Pekguleryuz, Surface characterization, in vitro and in vivo biocompatibility of Mg-0.3Sr-0.3Ca for temporary cardiovascular implant, Mater. Sci. Eng. C 67 (2016) 72–84.
[24] J.Y. Lock, E. Wyatt, S. Upadhyayula, A. Whall, V. Nunez, V.I. Vullev, H. Liu, Degradation and antibacterial properties of magnesium alloys in artificial urine for potential resorbable ureteral stent applications, J. Biomed. Mater. Res. A 102 (2014) 781–792.
[25] Q. Tian, C. Zhang, M. Deo, L. Rivera-Castaneda, N. Masoudipour, R. Guan, H. Liu, Responses of human urothelial cells to magnesium-zinc-strontium alloys and associated insoluble degradation products for urological stent applications, Mater. Sci. Eng. C 96 (2019) 248–262.
[26] X.X. Xu, F.L. Nie, Y.B. Wang, J.X. Zhang, W. Zheng, L. Li, Y.F. Zheng, Effective inhibition of the early copper ion burst release with ultra-fine grained copper and single crystal copper for intrauterine device application, Acta Biomater. 8 (2012) 886–896.
[27] R.A. Grayburn, M.G. Dowsett, P.J. Sabbe, D. Wermeille, J.A. Anjos, V. Flexer, M. De Keersmaecker, D. Wildermeersch, A. Adriaens, SR-XRD in situ monitoring of copper-IUD corrosion in simulated uterine fluid using a portable spectroelectrochemical cell, Bioelectrochemistry 110 (2016) 41–45.
[28] X. Cao, W. Zhang, X. Zhao, N. Lin, L. Wang, C. Li, L. Song, W. Zhang, Z. Zhang, D. Wildemeersch, Three-year efficacy and acceptability of the GyneFix® 200 intrauterine system, Contracept. 69 (2004) 207–211.
[29] C.M. March, Asherman's syndrome, Semin. Reprod. Med. 29 (2011) 83–94.
[30] Y.H. Lin, T.N. Jang, J.L. Hwang, L.W. Huang, K.M. Seow, B.C. Hsieh, C.H. Huang, Bacterial colonization with balloon uterine stent placement in the uterus for 30 days: a randomized controlled clinical trial, Fertil. Steril. 103 (2015) 513–518.
[31] C. Zhang, N. Xu, J. Lu, C. Ding, B. Yang, Study on corrosion of copper artificially formulated fluid for using electrochemical method, Reprod. Contracept. 12 (1995) 28–32.
[32] J. Wu, L. Wang, J. He, C. Zhu, In vitro cytotoxicity of Cu^{2+}, Zn^{2+}, Ag^{+} and their mixtures on primary human endometrial epithelial cells, Contracept. 85 (2012) 509–518.
[33] Z. Li, X. Gu, S. Lou, Y. Zheng, The development of binary Mg-Ca alloys for use as biodegradable materials within bone, Biomaterials 29 (2008) 1329–1344.
[34] S. Johnston, Z. Shi, A. Atrens, The influence of pH on the corrosion rate of high-purity Mg, AZ91 and ZE41 in bicarbonate buffered Hanks' solution, Corros. Sci. 101 (2015) 182–192.
[35] A.B. Johnson, R.F. Maness, R.G. Wheeler, Calcareous deposits formed on IUDs in human exposures, Contracept. 14 (1976) 507–517.
[36] A.B. Kar, A.D. Engineer, R. Goel, V.P. Kamboj, P.R. Dasgupta, S.R. Chowdhury, Effect of an intrauterine contraceptive device on biochemical composition of uterine fluid, Am. J. Obstet. Gynecol. 101 (1968) 966–970.
[37] L.G. Feo, The pH of the human uterine cavity in situ, Am. J. Obstet. Gynecol. 70 (1955) 60–64.
[38] S. Gaur, R.K. Singh Raman, A.S. Khanna, In vitro investigation of biodegradable polymeric coating for corrosion resistance of Mg-6Zn-Ca alloy in simulated body fluid, Mater. Sci. Eng. C Mater. Biol. Appl. 42 (2014) 91–101.
[39] R. Zeng, E. Han, W. Ke, A critical discussion on influence of loading frequency on fatigue crack propagation behavior for extruded Mg-Al-Zn alloys, Int. J. Fatigue 36 (2012) 40–46.
[40] R.C. Zeng, L. Sun, Y.F. Zheng, H.Z. Cui, E.H. Han, Corrosion and characterisation of dual phase Mg-Li-Ca alloy in Hank's solution: The influence of microstructural features, Corros. Sci. 79 (2014) 69–82.
[41] R.C. Zeng, Y. Hu, S.K. Guan, H.Z. Cui, E.H. Han, Corrosion of magnesium alloy AZ31: the influence of bicarbonate, sulphate, hydrogen phosphate and dihydrogen phosphate ions in saline solution, Corros. Sci. 86 (2014) 171–182.
[42] A. Yamamoto, S. Hiromoto, Effect of inorganic salts, amino acids and proteins on the degradation of pure magnesium in vitro, Mater. Sci. Eng. C 29 (2009) 1559–1568.
[43] N.T. Kirkland, J. Waterman, N. Birbilis, G. Dias, T.B. Woodfield, R.M. Hartshorn, M.P. Staiger, Buffer-regulated biocorrosion of pure magnesium, J. Mater. Sci. Mater. Med. 23 (2012) 283–291.
[44] K. Patai, M. Berényi, M. Sipos, B. Noszál, Characterization of Calcified Deposits on Contraceptive Intrauterine Devices, Contracept. 58 (1998) 305–308.
[45] Y. Liu, S. Zheng, N. Li, H. Guo, Y. Zheng, J. Peng, In vivo response of AZ31 alloy as biliary stents: a 6 months evaluation in rabbits, Sci. Rep. 7 (2017) 1–10.
[46] Z. Zou, W. Habraken, G. Matveeva, A.C.S. Jensen, L. Bertinetti, M.A. Hood, C.Y. Sun, P. Gilbert, I. Polishchuk, B. Pokroy, J. Mahamid, Y. Politi, S. Weiner, P. Werner, S. Bette, R. Dinnebier, U. Kolb, E. Zolotoyabko, P. Fratzl, A hydrated crystalline calcium carbonate phase: calcium carbonate hemihydrate, Sci. 363 (2019) 396-400.
[47] WHO. http://apps.who.int/iris/bitstream/10665/181468/1/9789241549158_eng.pdf?ua=1.
[48] A.K. Whitaker, L.K. Endres, S.Q. Mistretta, M.L. Gilliam, Postplacental insertion of the levonorgestrel intrauterine device after cesarean delivery vs. delayed insertion: a randomized controlled trial, Contracept. 89 (2014) 534–539.
[49] A. Sucak, S. Ozcan, S. Celen, T. Caglar, G. Goksu, N. Danisman, Immediate postplacental insertion of a copper intrauterine device: a pilot study to evaluate expulsion rate by mode of delivery, BMC Pregnancy Childbirth 15 (2015) 202.
[50] R.S.B. Howard, J. Tatum, Rebecca Ramos, Immediate postplacental insertion of GYNE-T 380 and GYNE-T 380 Postpartum intrauterine contraceptive devices: randomized study, Am. J. Obstet. Gynecol. 175 (1996) 1231–1235.
[51] http://www.hjmed.com/contents/31/44.html.
[52] M.L. Houchin, E.M. Topp, Physical properties of PLGA films during polymer degradation, J. Appl. Polym. Sci. 114 (2009) 2848–2854.
[53] M. Jamshidian, E.A. Tehrany, M. Imran, M. Jacquot, S. Desobry, Poly-Lactic Acid: Production, Applications, Nanocomposites, and Release Studies, Compr. Rev. Food Sci. Food Saf. 9 (2010) 552–571.
[54] D. Bian, W. Zhou, Y. Liu, N. Li, Y. Zheng, Z. Sun, Fatigue behaviors of HP-Mg, Mg-Ca and Mg-Zn-Ca biodegradable metals in air and simulated body fluid, Acta Biomater. 41 (2016) 351–360.
[55] S.K. Munro, C.M. Farquhar, M.D. Mitchell, A.P. Ponnampalam, Epigenetic regulation of endometrium during the menstrual cycle, Mol. Hum. Reprod. 16 (2010) 297–310.
[56] J. Choi, M. Jo, E. Lee, D.Y. Lee, D. Choi, Involvement of endoplasmic reticulum stress in regulation of endometrial stromal cell invasiveness: possible role in pathogenesis of endometriosis, Mol. Hum. Reprod. 25 (2019) 101–110.
[57] A. Freis, T. Renke, U. Kammerer, J. Jauckus, T. Strowitzki, A. Germeyer, Effects of a hyperandrogenaemic state on the proliferation and decidualization potential in human endometrial stromal cells, Arch. Gynecol. Obstet. 295 (2017) 1005–1013.

[58] E. Zhang, L. Xu, G. Yu, F. Pan, K. Yang, In vivo evaluation of biodegradable magnesium alloy bone implant in the first 6 months implantation, J. Biomed. Mater. Res. A 90 (2009) 882–893.

[59] C.D. Zhang, N.X. Xu, J.F. Lu, C.H. Ding, Study on corrosion of copper in artificially formulated fluid using electrochemical method, Reprod. Contracept. 15 (1995) 28–32.

[60] T. Kokubo, H. Takadama, How useful is SBF in predicting in vivo bone bioactivity?, Biomaterials 27 (2006) 2907–2915

[61] Ayako Oyane, Hyun-Min Kim, Takuo Furuya, Tadashi Kokubo, Toshiki Miyazaki, T. Nakamura, Preparation and assessment of revised simulated body fluids, J. Biomed. Mater. Res. A 65 (2003) 188–195.

[62] Y.F. Zheng, X.N. Gu, Y.L. Xi, D.L. Chai, In vitro degradation and cytotoxicity of Mg/Ca composites produced by powder metallurgy, Acta Biomater. 6 (2010) 1783–1791.

[63] L.Y. Qiao, J.C. Gao, Y. Wang, S.L. Wang, S. Wu, Y. Xue, Biocompatibility Evaluation of Magnesium-Based Materials, Mater. Sci. Forum (2007) 459–462.

[64] F.A.-Y. Abbas, T. Kobra, M.M.H. Seyed, T.-K. Tahereh, R. Mahboobeh, M.A. Seyedeh, S.M. Maryam, Cytotoxicity assessment of adipose-derived mesenchymal stem cells on synthesized biodegradable Mg-Zn-Ca alloys, Mater. Sci. Eng. C Mater. Biol. Appl. 69 (2016) 584–597.

[65] S. Zhang, X. Zhang, C. Zhao, J. Li, Y. Song, C. Xie, H. Tao, Y. Zhang, Y. He, Y. Jiang, Y. Bian, Research on an Mg-Zn alloy as a degradable biomaterial, Acta Biomater. 6 (2010) 626–640.

[66] J. Kubásek, D. Vojtěch, Structural characteristics and corrosion behavior of biodegradable Mg–Zn, Mg–Zn–Gd alloys, J. Mater. Sci.: Mater. Med. 24 (2013) 1615–1626.

[67] Y. Yan, Y. Kang, D. Li, K. Yu, T. Xiao, Y. Deng, H. Dai, Y. Dai, H. Xiong, H. Fang, Improvement of the mechanical properties and corrosion resistance of biodegradable β-$Ca_3(PO_4)_2$ /Mg-Zn composites prepared by powder metallurgy: the adding β-$Ca_3(PO_4)_2$, hot extrusion and aging treatment, Mater. Sci. Eng. C 74 (2017) 582–596.